In situ synthesis of Zn2GeO4 hollow spheres and their enhanced photocatalytic activity for the degradation of antibiotic metronidazole

ARTICLE *in* DALTON TRANSACTIONS · FEBRUARY 2013

Impact Factor: 4.2 · DOI: 10.1039/c2dt32623j · Source: PubMed

4 AUTHORS, INCLUDING:

Gaoke Zhang
Wuhan University of Technology
182 PUBLICATIONS **2,239** CITATIONS

SEE PROFILE

Dalton Transactions

RSC Publishing

PAPER

In situ synthesis of Zn_2GeO_4 hollow spheres and their enhanced photocatalytic activity for the degradation of antibiotic metronidazole

Cite this: *Dalton Trans.*, 2013, **42**, 5092

Jin Liu,[a] Gaoke Zhang,*[a] Jimmy C. Yu*[a,b] and Yadan Guo[a]

Received 2nd November 2012,
Accepted 3rd January 2013

DOI: 10.1039/c2dt32623j

www.rsc.org/dalton

In this study, Zn_2GeO_4 hollow spheres were successfully fabricated by a template-engaged approach using zinc hydroxide carbonate ($Zn_4CO_3(OH)_6{\cdot}H_2O$, ZHC) spheres as the template. During the hydrothermal process, Zn^{2+} dissolved from the surface of the ZHC spheres could rapidly react with the $HGeO_3^-$ in solution and the Zn_2GeO_4 outer shell was formed *in situ*. Moreover, the building units of the Zn_2GeO_4 hollow spheres could gradually transform from the nanoparticles into nanobundles with the increase of the reaction time. The photocatalytic degradation results indicate that the Zn_2GeO_4 hollow spheres exhibited high photocatalytic activity and excellent stability for the degradation of antibiotic metronidazole in solution. Finally, the radical species involved in the degradation process have been investigated by using the scavenger experiments.

Introduction

Three-dimensional (3D) hollow materials have been studied in hydrogen storage, high-energy batteries, sensors and catalytic fields.[1–5] In recent years, 3D hollow spheres have attracted increasing attention due to their potential application in photocatalysis. The high photocatalytic activities of the hollow spheres are mostly attributed to their large surface area and open hollow structure, which enable both the outer and inner surfaces of the catalyst to come into contact with the reactants, yielding added benefits for the catalytic process.[6,7] Hollow spheres can also effectively enhance light harvesting efficiency by simultaneously increasing the diffractions on the hollow spheres and the reflections on the shell structure.[8] Generally, the most common methods for the synthesis of hollow spheres are template-based ones, including soft template methods using organic surfactants or hard template methods using solid templates. Ostwald ripening and the Kirkendall effect based methods have also been developed to fabricate hollow structures.[9] However, for complicated structures such as ternary oxide, the capabilities of the template and template-free approaches are limited. So far little progress has been reported on the synthesis of germanate compounds with hollow spheres.

Zn_2GeO_4, as a ternary oxide with the willemite structure, has attracted great attention for various applications due to its optical and electrochemical properties.[10–12] A Zn_2GeO_4 crystal cell is composed of GeO_4 tetrahedra and ZnO_4 tetrahedra. A GeO_4 tetrahedron of Zn_2GeO_4 is so heavily distorted to generate a dipole moment inside, which is considered to promote the separation of electron–hole pairs generated by light irradiation.[13] Owing to its intrinsic properties such as stability, electronic configuration and crystal structure, Zn_2GeO_4 can be used as a promising photocatalyst for photoreduction of CO_2 and decomposition of water and organic pollutants.[14–16] It is worth noting that all of the dielectric, piezoelectric, and photocatalytic properties strongly depend on the crystal structure and morphology. Therefore, many efforts have been made for the controllable preparation of special microstructures. Up to now, several solution routes and gas phase evaporation techniques have been developed to prepare Zn_2GeO_4 with one-dimensional and two-dimensional nanostructures, such as nanorods, nanobelts, nanobundles and nanowires.[17–20] To the best of our knowledge, no work has been reported on the synthesis of 3D Zn_2GeO_4 hollow spheres.

In this paper, we firstly developed a template-engaged approach for the synthesis of Zn_2GeO_4 hollow spheres by using $Zn_4CO_3(OH)_6{\cdot}H_2O$ spheres as sacrificial templates and GeO_2 as the precursor under hydrothermal conditions. The influence of reaction time on the formation of the Zn_2GeO_4 hollow spheres was systematically investigated. The photocatalytic activity of the Zn_2GeO_4 hollow spheres has been evaluated

[a]*School of Resources and Environmental Engineering, Wuhan University of Technology, Wuhan, 430070, China. E-mail: gkzhang@whut.edu.cn; Fax: +86-27-87887445; Tel: +86-27-87651816*

[b]*Department of Chemistry and Institute of Environment, Energy and Sustainability, The Chinese University of Hong Kong, ShatinNew Territories, Hong Kong, China. E-mail: jimyu@cuhk.edu.hk; Fax: +852-2603-5057; Tel: +852-3943-6268*

by the degradation of antibiotic metronidazole as a model organic pollutant and the Zn_2GeO_4 hollow spheres exhibited high photocatalytic activity and excellent stability. The effects of the involved active species in the photocatalytic process were also discussed in detail.

Experimental section

Synthesis of zinc carbonate hydroxide spheres

Zinc nitrate hexahydrate ($Zn(NO_3)_2{\cdot}6H_2O$, SCRC, China), urea ($CO(NH_2)_2$, SCRC, China), and trisodium citrate ($C_6H_5Na_3O_7{\cdot}2H_2O$, SCRC, China) used in the experiments were of analytical grade and used without further purification. Zinc hydroxide carbonate ($Zn_4CO_3(OH)_6{\cdot}H_2O$, ZHC) spheres were synthesized by a hydrothermal method reported by Zou *et al.*[21] In a typical synthesis, 0.446 g zinc nitrate hexahydrate, 0.182 g urea and 0.044 g trisodium citrate were firstly dissolved in 30 mL deionized water with stirring. Then, the mixture solution was transferred into a 50 mL Teflon-lined stainless steel autoclave and heated at 120 °C for 6 h in a digital-type temperature-controlled oven. After being cooled to room temperature, the white precipitate was collected, centrifuged, washed with deionized water five times, and dried at 70 °C.

Synthesis of Zn_2GeO_4 catalysts

Germanium(IV) oxide (GeO_2, SCRC, China) and zinc oxide (ZnO, SCRC, China) used in the experiments are of analytical purity and used without further purification. In a typical synthesis, 0.274 g ZHC and 0.130 g GeO_2 were mixed with 35 mL of deionized water. The mixture was then transferred into a 50 mL Teflon-lined stainless steel autoclave and heated at 200 °C for different times in a digital-type temperature-controlled oven and then cooled to room temperature. After the hydrothermal reaction, the samples were collected, centrifuged, and washed with deionized water five times. Finally the white powders were obtained by drying at 70 °C. A reference Zn_2GeO_4 sample (SSR-Zn_2GeO_4) was prepared by the solid-state reaction of ZnO and GeO_2 (mass ratio of 1 : 2) at 1200 °C for 16 h in air.

Characterization

The structure and crystallinity of the as-prepared samples were characterized by powder X-ray diffraction (XRD) analysis on a D/MAX-RB diffractometer with Cu Kα radiation under the operation conditions of 40 kV and 50 mA. X-ray photoelectron spectroscopy (XPS) analysis was carried out by using a Thermo VG Multilab 2000 spectrometer (UK) with a monochromatic Al Kα source. All binding energies were referenced to the C 1s peak at 284.63 eV of the surface adventitious carbon and revised. Scanning electron microscopy (SEM, JSM-5610LV) and field emission scanning electron microscopy (FESEM, S-4800) were used to characterize the morphologies of the samples. The morphologies and microstructures of the prepared samples were further examined by transmission electron microscopy (TEM) and high-resolution transmission electron microscopy (HRTEM) using a JEM 2100F electron microscope operated at an accelerating voltage of 200 kV. The Brunauer–Emmett–Teller (BET) specific surface areas of the powders were obtained by nitrogen adsorption on an Autosorb-1 (Quantachrome Instruments, Boynton Beach, Florida) nitrogen adsorption apparatus. A Nexus Fourier transform infrared (FT-IR) spectroscope (Thermo Nicolet, USA) was used to detect the chemical bonds of the composite. The absorption edges of the samples were measured by a UV-vis spectrophotometer (UV2550, Shimadzu Corporation, Kyoto, Japan). $BaSO_4$ was used as a reflectance standard.

Photocatalytic activity measurements

The photocatalytic activities of the as-obtained Zn_2GeO_4 samples were evaluated by the photocatalytic degradation of metronidazole in aqueous solution. In each experiment, 0.1 g of the Zn_2GeO_4 samples was dispersed in 100 mL of metronidazole aqueous solution (10 mg L^{-1}). Prior to UV light illumination, the suspension was vigorously stirred in the dark for 20 min. The irradiation was performed with a 20 W UV light lamp (λ = 253.7 nm). The distance between the light source and the bottom of the solution was about 12 cm. The light intensity was about 0.750 mW cm^{-2} measured by a UV-B radiometer. At given time intervals, about 8 mL of the suspension was taken out and centrifuged to remove the photocatalyst particles. The concentration of the metronidazole solution was analyzed using a UV-vis spectrophotometer (UV1750, Shimadzu Corporation, Japan). The stability of the Zn_2GeO_4 hollow spheres was also evaluated by reusing the catalyst for five runs for the degradation of metronidazole under the same conditions.

Results and discussion

Structure and morphology

Fig. 1 shows the XRD patterns of the $Zn_4CO_3(OH)_6{\cdot}H_2O$ spheres template and the Zn_2GeO_4 hollow spheres (200 °C, 5 h). From Fig. 1a, it can be seen that all the reflection peaks could be indexed to a pure $Zn_4CO_3(OH)_6{\cdot}H_2O$ (JCPDS 11-0287). The Zn_2GeO_4 hollow spheres were prepared by a template-engaged method. The XRD pattern of the final sample (Fig. 1b) could be well indexed to the pure Zn_2GeO_4 (JCPDS 11-0687).

The surface element composition and chemical state of the Zn_2GeO_4 hollow spheres were confirmed by XPS analysis (Fig. 2). Fig. 2 shows the XPS spectra of Zn 2p and Ge 3d of the Zn_2GeO_4 hollow spheres. As shown in Fig. 2a, the peaks centered at 1021.9 and 1044.9 eV are attributed to Zn $2p_{3/2}$ and Zn $2p_{1/2}$, which reveal the oxidation state of Zn^{2+} in the sample.[22] From Fig. 2b, the peak at 32.1 eV is assigned to Ge 3d, indicating that germanium in the sample exists in the form of Ge^{4+}.[23]

The morphology and microstructure of the as-prepared samples were investigated by SEM and TEM. A typical image of the ZHC precursor obtained by SEM is shown in Fig. 3a. It is shown that the precursor is composed of relatively uniform

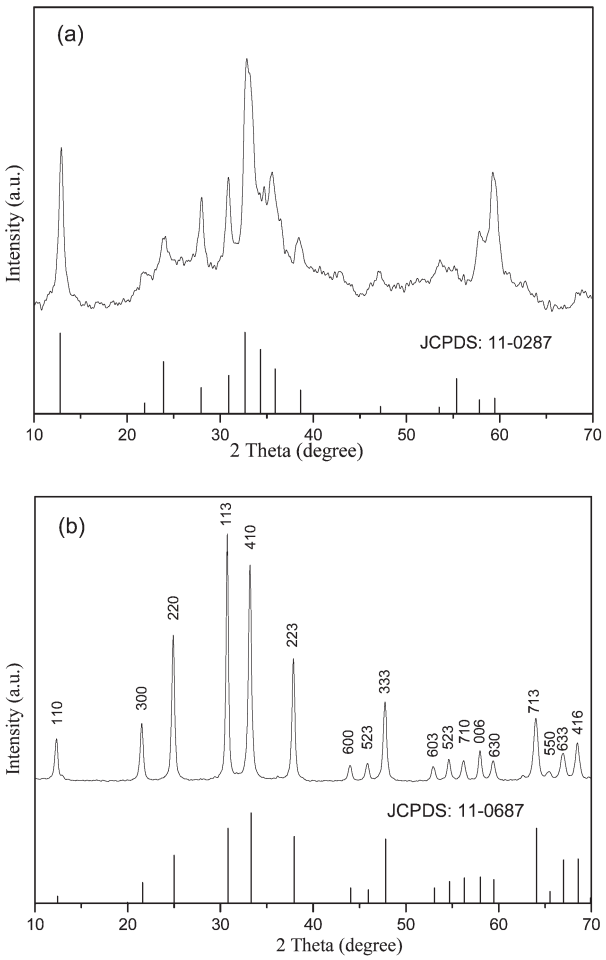

Fig. 1 XRD patterns of the (a) $Zn_4CO_3(OH)_6{\cdot}H_2O$ spheres and (b) Zn_2GeO_4 hollow spheres synthesized for 5 h.

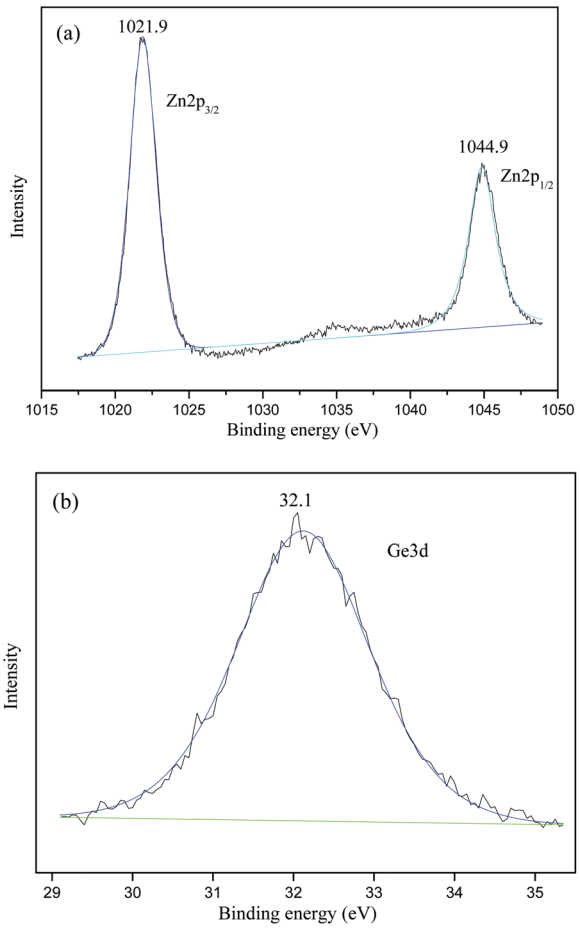

Fig. 2 XPS spectra of Zn_2GeO_4 hollow spheres: (a) Zn 2p and (b) Ge 3d.

ZHC spheres with diameters in the range of 5–10 μm. Fig. 3b indicates that the spheres have a honeycomb structure, constructed by many inter-connected nanosheets, providing lots of channels for the diffusion of the Zn^{2+}. From Fig. 3c and d, it can be seen that Zn_2GeO_4 hollow spheres are composed of abundant nanobundles constructed by nanorods 400–600 nm in length and 30–50 nm in width.

To get more detailed information about the hollow structure, TEM and HRTEM measurements were carried out. The hollow structure of Zn_2GeO_4 spheres was further observed by the typical TEM images (Fig. 4a and b). Well-resolved lattice fringes are clearly visible (Fig. 4c and d), with an interplanar *d* spacing of 0.269 nm corresponding to the (410) lattice planes of the rhombohedral Zn_2GeO_4 structure, indicating good crystallization of the Zn_2GeO_4 hollow spheres.

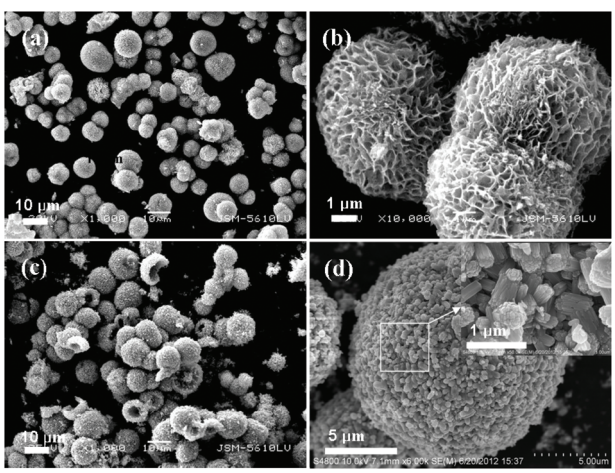

Fig. 3 SEM images of (a, b) ZHC spheres and (c, d) Zn_2GeO_4 hollow spheres synthesized at 200 °C for 5 h. The inset of (d) shows the enlarged image of the corresponding area.

N_2 adsorption–desorption

To further investigate information on the surface area and pores in the Zn_2GeO_4 hollow spheres (200 °C, 5 h), nitrogen adsorption measurement was employed, and the corresponding results are presented in Fig. 5. The shape of the isotherm seems to be nearly type IV with a hysteresis cycle type H3 according to the IUPAC classification.[24,25] The inset of Fig. 5 shows the pore size distribution curve calculated by the BJH method from the adsorption branch of a nitrogen isotherm. The micropores and mesopores are associated with the

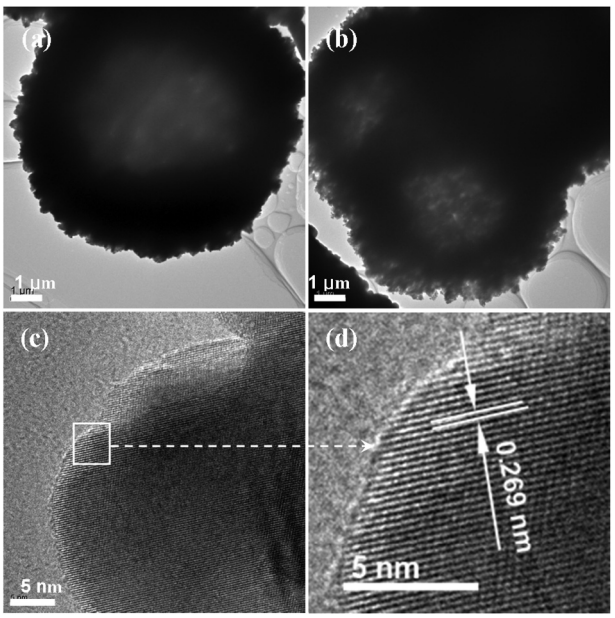

Fig. 4 TEM and HRTEM images of Zn_2GeO_4 hollow spheres synthesized at 200 °C for 5 h.

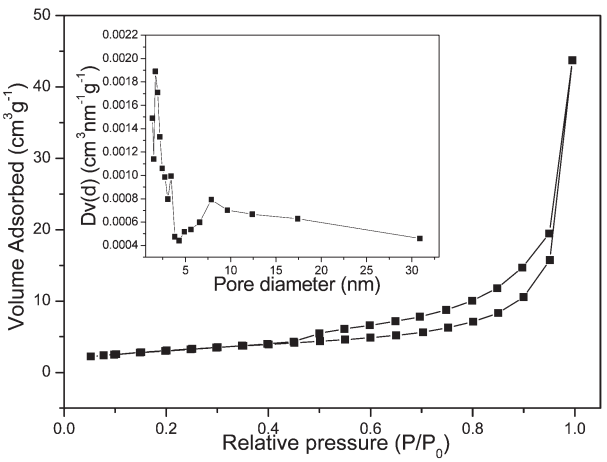

Fig. 5 Nitrogen adsorption–desorption isotherm and pore size distribution (inset) of the Zn_2GeO_4 hollow spheres.

agglomeration of Zn_2GeO_4 nanobundles. The surface area of the Zn_2GeO_4 hollow spheres determined by the BET method was 11.05 $m^2\ g^{-1}$.

Possible formation process of Zn_2GeO_4 hollow spheres

In order to understand the formation process of the Zn_2GeO_4 hollow spheres, time-dependent experiments were carried out. The samples collected at different stages were investigated by SEM (Fig. 6) and XRD (Fig. 7). Fig. 6 shows SEM images of the Zn_2GeO_4 samples obtained for different reaction times. After hydrothermal treatment for 40 min, a Zn_2GeO_4 core–shell structure was formed (Fig. 6a). From the inset of Fig. 6a, it can be seen that the core was the $Zn_4CO_3(OH)_6{\cdot}H_2O$ template. When the reaction time was prolonged to 1 h, the Zn_2GeO_4

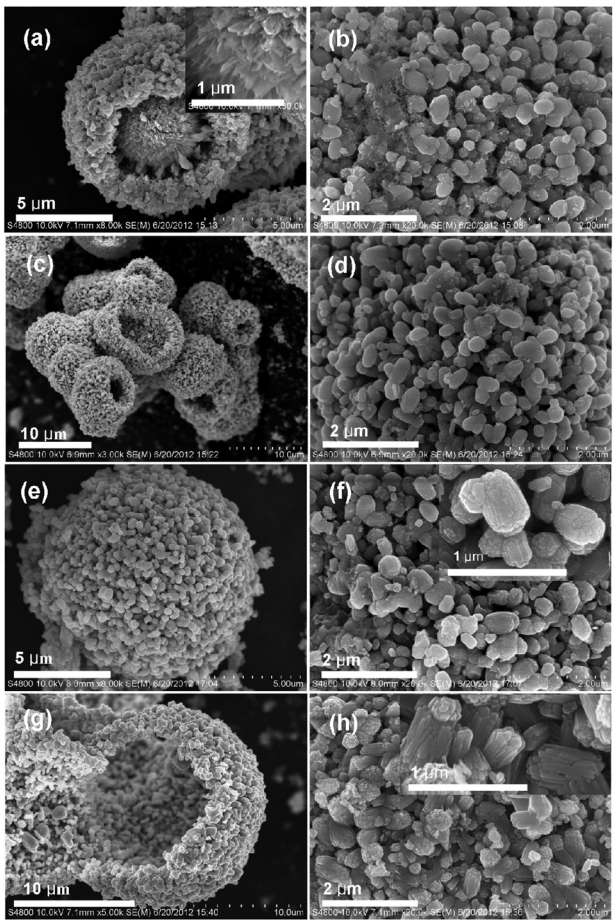

Fig. 6 FESEM images of the Zn_2GeO_4 samples synthesized for different reaction times: (a, b) 40 min, (c, d) 1 h, (e, f) 2 h and (g, h) 5 h. Insets of (a, f, h) show the enlarged images of the corresponding spheres.

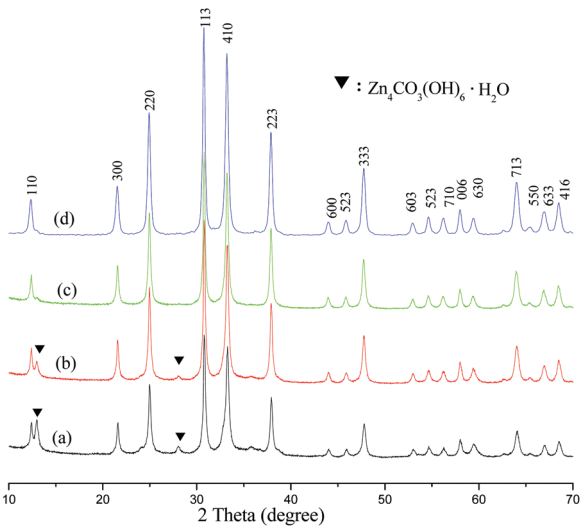

Fig. 7 XRD patterns of the Zn_2GeO_4 samples synthesized for different reaction times: (a) 40 min, (b) 1 h, (c) 2 h and (d) 5 h.

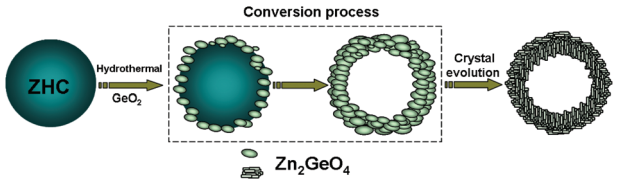

Fig. 8 Schematic illustration of the possible formation process of the Zn_2GeO_4 hollow spheres.

core–shell structure disappeared and the hollow structures were formed (Fig. 6c). From Fig. 6b and d, it can be seen that the Zn_2GeO_4 shell is assembled by nanoparticles 200–400 nm in size. The corresponding XRD patterns imply that the sample was a mixed phase of Zn_2GeO_4 (JCPDS 11-0687) and $Zn_4CO_3(OH)_6{\cdot}H_2O$ (JCPDS 11-0287) (Fig. 7a and b). When the reaction time was increased to 2 h, no other impurities could be observed (Fig. 7c). The nanobundles constructed of many nanorods could be obviously observed on the surface of Zn_2GeO_4 hollow spheres and these nanorod building blocks were arranged side by side and bound tightly (Fig. 6e and f). By further increasing the reaction time to 5 h, the nanorods increased to 400–600 nm in length (Fig. 6g and h) and the diffraction peak intensity became stronger, demonstrating that the degree of crystallization of the Zn_2GeO_4 hollow spheres increased. From the time-dependent experiments, it can be concluded that the possible reactions involved in the reaction process could be summarized by eqn (1)–(3).[18,26]

$$GeO_2 + H_2O \rightarrow HGeO_3^- + H^+ \quad (1)$$

$$Zn_4CO_3(OH)_6 \cdot H_2O \rightarrow 4Zn^{2+} + CO_3^{2-} + 6OH^- + H_2O \quad (2)$$

$$2Zn^{2+} + HGeO_3^- + H_2O \rightarrow Zn_2GeO_4 + 3H^+ \quad (3)$$

On the basis of the above experimental results, we proposed the possible formation process of Zn_2GeO_4 hollow spheres (Fig. 8). Zn^{2+} dissolved from the surface of the ZHC spheres could rapidly react with the $HGeO_3^-$ in solution and the Zn_2GeO_4 outer shell was formed *in situ* and the spherical morphology was well preserved. Then, a direct chemical reaction was hindered and further reaction depended on the outdiffusion rate of Zn^{2+} and the interdiffusion rate of $HGeO_3^-$ through this interface. The Zn_2GeO_4 hollow spheres would be formed until Zn^{2+} completely diffused outward through the Zn_2GeO_4 shell and reacted with $HGeO_3^-$ in solution. Therefore, it can be deduced that the Zn_2GeO_4 hollow spheres were formed by the template-engaged approach.[27–31] On the other hand, it was noted that the building units of the Zn_2GeO_4 hollow spheres could gradually transform from nanoparticles into nanobundles with the increase of the reaction time.

UV-vis diffuse reflectance spectra

Fig. 9 shows the UV-vis diffuse reflectance spectra of the Zn_2GeO_4 hollow spheres (200 °C, 5 h). From Fig. 9, it can be seen that the wavelength of the optical absorption edge of the Zn_2GeO_4 hollow spheres is about 276 nm. The band gap of

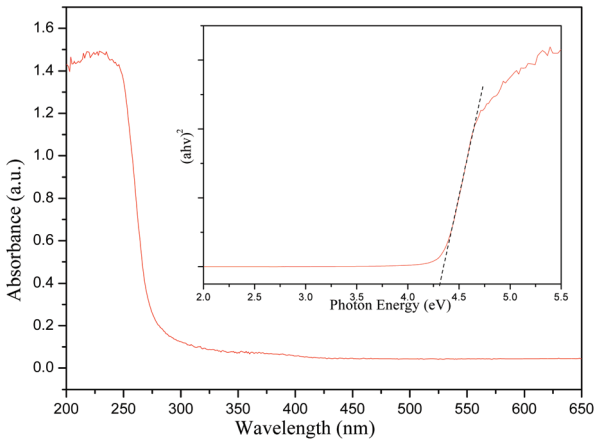

Fig. 9 UV-vis diffuse reflectance spectra of the Zn_2GeO_4 hollow spheres.

Zn_2GeO_4 hollow spheres is estimated as 4.3 eV based on eqn (4).[32]

$$ah\nu = A(h\nu - E_g)^{n/2} \quad (4)$$

where a, ν, A, and E_g are the absorption coefficient, light frequency, proportionality constant, and band gap, respectively. Here n is equal to 1 as Zn_2GeO_4 is a direct gap semiconductor.[18,33]

Photocatalytic degradation

Metronidazole is a kind of nitroimidazole antibiotic, which is commonly used in clinical applications and widely used for the treatment of infectious diseases. Because of its potentially carcinogenic and mutagenic nature, metronidazole must be completely eliminated from the effluent of the wastewater treatment plant before discharging. Nevertheless, it is difficult to remove metronidazole by traditional methods due to its low biodegradability and high solubility in water. Thus, the photocatalytic degradation of metronidazole was chosen to investigate the photocatalytic activity of the as-prepared photocatalyst.[34,35] Fig. 10a displays the UV-vis absorption spectra of antibiotic metronidazole solution during photocatalytic degradation by the Zn_2GeO_4 hollow spheres. The absorption spectra of the metronidazole solution show a characteristic peak at 320 nm. The intensity of the absorption peak at 320 nm decreased gradually with increasing UV exposure time and the absorption peak almost disappeared after 80 min, which meant that the metronidazole was destroyed. Fig. 10b displays the degradation of metronidazole solution under different conditions. As shown in Fig. 10b, about 5% of metronidazole was photolyzed after 80 min in the absence of photocatalyst. However, almost 100% of metronidazole was degraded on the Zn_2GeO_4 hollow spheres after 80 min irradiation. The adsorption of metronidazole on the Zn_2GeO_4 hollow spheres in the dark was also checked and the adsorption of metronidazole was negligible, suggesting that the degradation of metronidazole was caused by photodegradation but not adsorption under UV light irradiation. From Fig. 10b,

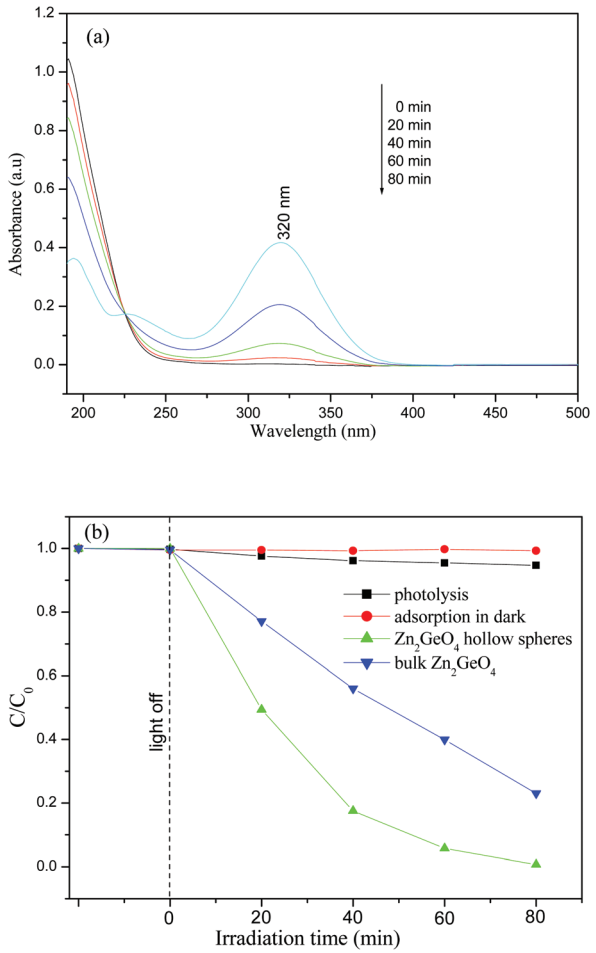

Fig. 10 (a) UV-vis absorption spectra of metronidazole solution during photocatalytic degradation by the Zn_2GeO_4 hollow spheres, (b) degradation of metronidazole solution under different conditions.

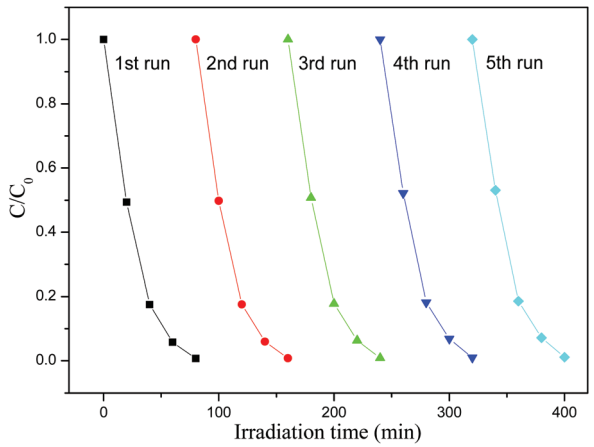

Fig. 11 Cycling runs of the Zn_2GeO_4 hollow spheres for the degradation of metronidazole solution.

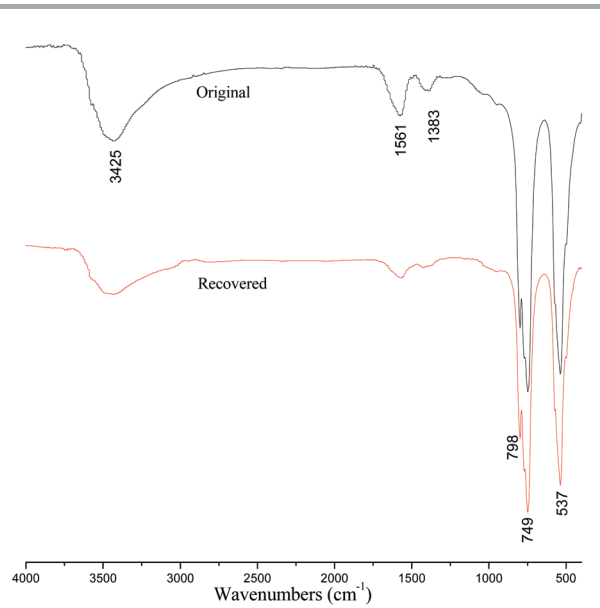

Fig. 12 FT-IR spectra of Zn_2GeO_4 hollow spheres before and after the photocatalytic degradation of metronidazole solution.

it can be seen that the Zn_2GeO_4 hollow spheres showed excellent photocatalytic activity compared to the SSR-Zn_2GeO_4. The higher photocatalytic property of the Zn_2GeO_4 hollow spheres could be ascribed to the hollow structure and high specific surface area (Zn_2GeO_4 hollow spheres: 11.05 $m^2\ g^{-1}$; SSR-Zn_2GeO_4: 0.0025 $m^2\ g^{-1}$), which increased more light harvesting efficiency and reaction sites.

The Zn_2GeO_4 hollow spheres can be easily recycled by a simple sedimentation without further treatment. As shown in Fig. 11, after five recycles for the photocatalytic degradation of metronidazole, the Zn_2GeO_4 hollow spheres did not exhibit any significant loss of photocatalytic activity. The corresponding FT-IR results (Fig. 12) show that there is no observable structural difference between the Zn_2GeO_4 hollow spheres before and after photocatalytic degradation of metronidazole. The absorption peaks of the samples observed at 799, 749 and 535 cm^{-1} are associated with vibration modes of the ZnO_4 and GeO_4 tetrahedron, respectively, in Zn_2GeO_4.[36] The absorption peaks at 3426, 1561 and 1383 cm^{-1} are attributed to the vibrations of the H_2O, COO^- and NO_3^-, respectively.[37,38] These results suggest that the Zn_2GeO_4 hollow spheres have excellent stability and do not suffer from photocorrosion during the degradation process.

To further investigate the effect of the involved active species in the photocatalytic process, a series of quenchers were developed to scavenge the relevant species and their concentration is about 2.0 mM. The comparison experiments were performed without quenchers under identical conditions. The results of metronidazole degradation efficiency with different quenchers are shown in Fig. 13. The quenchers used in this study were potassium iodide (KI) for h^+ and $^{\cdot}OH$, sodium oxalate ($Na_2C_2O_4$) for h^+, benzoquinone (BQ) for $^{\cdot}O_2^-$ and isopropanol (IPA) for $^{\cdot}OH$.[39–42] It can be observed that $Na_2C_2O_4$ had a little influence on the metronidazole degradation, indicating that h^+ on the surface of the Zn_2GeO_4 catalyst did not play a major role in the photodegradation system. However, the degradation efficiency decreased obviously after the

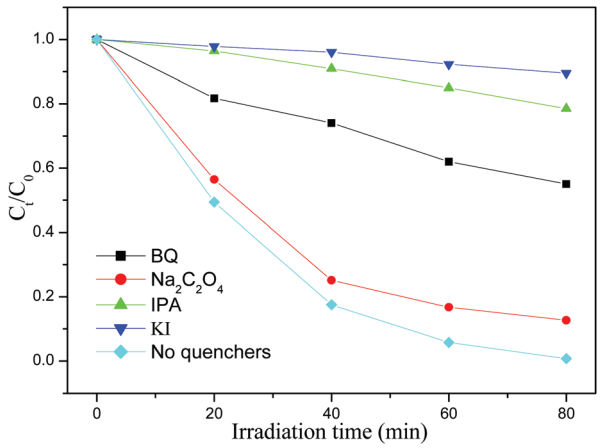

Fig. 13 Photocatalytic degradation of metronidazole solution over the Zn_2GeO_4 hollow spheres with or without the quenchers under UV light irradiation.

addition of KI, IPA or BQ, indicating that $^{\cdot}OH$ and $^{\cdot}O_2^-$ were produced and acted as dominating reactive species in the metronidazole degradation under UV light irradiation.

Conclusions

In summary, the Zn_2GeO_4 hollow spheres were successfully synthesized by using $Zn_4CO_3(OH)_6{\cdot}H_2O$ spheres as the template under hydrothermal conditions. The morphology and size of the building units of the Zn_2GeO_4 hollow spheres could be easily controlled by adjusting the reaction time. Owing to the hollow structure and high specific surface area, the Zn_2GeO_4 hollow spheres exhibited high photocatalytic properties and excellent stability for the degradation of metronidazole compared to SSR-Zn_2GeO_4. The results demonstrate that the Zn_2GeO_4 hollow spheres are promising photocatalysts for the degradation of antibiotic metronidazole.

Acknowledgements

This work was supported by the National Basic Research Program of China (973 Program) 2013CB632402, SRFDP (20110143110015), the National Key Technology R&D Program of China (2012BAJ25B02-03) and the Program of Wuhan Subject Chief Scientist (201150530147). We also gratefully acknowledge the assistance of Prof. J. G. Yu at the State Key Laboratory of Advanced Technology for Materials Synthesis and Processing (Wuhan University of Technology, P. R. China).

Notes and references

1 B. Z. Fang, M. Kim, J. H. Kim and J. S. Yu, *Langmuir*, 2008, **24**, 12068.
2 X. W. Lou, Y. Wang, C. L. Yuan, J. Y. Lee and L. A. Archer, *Adv. Mater.*, 2006, **18**, 2325.
3 S. J. Guo and E. Wang, *Acc. Chem. Res.*, 2011, **44**, 491.
4 L. S. Zhong, J. S. Hu, A. M. Cao, Q. Liu, W. G. Song and L. J. Wan, *Chem. Mater.*, 2007, **19**, 1648.
5 J. X. Xia, S. Yin, H. M. Li, H. Xu, L. Xu and Y. G. Xu, *Dalton Trans.*, 2011, **40**, 5249.
6 Z. K. Zheng, B. B. Huang, X. Y. Qin, X. Y. Zhang and Y. Dai, *J. Colloid Interface Sci.*, 2011, **358**, 68.
7 L. Zhou, W. Z. Wang, H. L. Xu and S. M. Sun, *Cryst. Growth Des.*, 2008, **8**, 3595.
8 X. Y. Lai, J. E. Halpert and D. Wang, *Energy Environ. Sci.*, 2012, **5**, 5604.
9 X. W. Lou, L. A. Archer and Z. C. Yang, *Adv. Mater.*, 2008, **20**, 3987.
10 M. Y. Tsai, C. Y. Yu, C. C. Wang and T. P. Perng, *Cryst. Growth Des.*, 2008, **8**, 2264.
11 S. Takeshita, J. Honda, T. Isobe, T. Sawayama and S. Niikura, *Cryst. Growth Des.*, 2010, **10**, 4494.
12 M. M. Jumidali, K. M. Sulieman and M. R. Hashim, *Appl. Surf. Sci.*, 2011, **257**, 4890.
13 J. Sato, H. Kobayashi, K. Ikarashi, N. Saito, H. Nishiyama and Y. Ioue, *J. Phys. Chem. B*, 2004, **108**, 4369.
14 B. J. Ma, F. Y. Wen, H. F. Jiang, J. H. Yang, P. L. Ying and C. Li, *Catal. Lett.*, 2010, **134**, 78.
15 J. H. Huang, X. C. Wang, Y. D. Hou, X. F. Chen, L. Wu and X. Z. Fu, *Environ. Sci. Technol.*, 2008, **42**, 7387.
16 N. Zhang, S. X. Ouyang, P. Li, Y. J. Zhang, G. C. Xi, T. Kako and J. H. Ye, *Chem. Commun.*, 2011, **47**, 2041.
17 Q. Liu, Y. Zhou, J. H. Kou, X. Y. Chen, Z. P. Tian, J. Gao, S. C. Yan and Z. G. Zou, *J. Am. Chem. Soc.*, 2010, **132**, 14385.
18 J. H. Huang, K. N. Ding, Y. D. Hou, X. C. Wang and X. F. Fu, *ChemSusChem*, 2008, **1**, 1011.
19 L. Zhang, X. F. Cao, Y. L. Ma, X. T. Chen and Z. L. Xue, *CrystEngComm*, 2010, **12**, 3201.
20 C. Y. Yan and P. S. Lee, *J. Phys. Chem. C*, 2010, **114**, 265.
21 A. Lei, B. H. Qu, W. C. Zhou, Y. G. Wang, Q. L. Zhang and B. S. Zou, *Mater. Lett.*, 2012, **66**, 72.
22 J. B. Mu, C. L. Shao, Z. C. Guo, Z. Y. Zhang, M. Y. Zhang, P. Zhang, B. Chen and Y. C. Liu, *ACS Appl. Mater. Interfaces*, 2011, **3**, 590.
23 Y. G. Lee, K. Teramura, M. Hara and K. Domen, *Chem. Mater.*, 2007, **19**, 2120.
24 F. Z. Shi, Y. G. Li, H. Z. Wang and Q. H. Zhang, *Appl. Catal., B*, 2012, **123–124**, 127.
25 S. A. K. Leghari, S. Sajjad, F. Chen and J. L. Zhang, *Chem. Eng. J.*, 2011, **166**, 906.
26 C. L. Yan and D. F. Xue, *J. Phys. Chem. B*, 2006, **110**, 7102.
27 P. F. Zuo, S. Y. Zhang, B. K. Jin, Y. P. Tian and J. X. Yang, *J. Phys. Chem. C*, 2008, **112**, 14825.
28 Z. Y. Wang, D. Y. Luan, C. M. Li, F. B. Su, S. Madhavi, F. Y. C. Boey and X. W. Lou, *J. Am. Chem. Soc.*, 2010, **132**, 16271.
29 Z. Y. Wang, D. Y. Luan, F. Y. C. Boey and X. W. Lou, *J. Am. Chem. Soc.*, 2011, **133**, 4738.

30 L. Zhang, L. Zhou, H. B. Wu, R. Xu and X. W. Lou, *Angew. Chem., Int. Ed.*, 2012, **51**, 7267.
31 L. Zhou, D. Y. Zhao and X. W. Lou, *Adv. Mater.*, 2012, **24**, 745.
32 J. W. Tang, Z. G. Zou and J. H. Ye, *J. Phys. Chem. C*, 2003, **107**, 14265.
33 Q. Liu, Y. Zhou, Z. P. Tian, X. Y. Chen, J. Gao and Z. G. Zou, *J. Mater. Chem.*, 2012, **22**, 2033.
34 Z. Q. Fang, X. Q. Qiu, J. H. Chen and X. H. Qiu, *Appl. Catal., B*, 2010, **100**, 211.
35 M. Sánchez-Polo, J. Rivera-Utrilla, G. Prados-Joya, M. A. Ferro-García and I. Bautista-Toledo, *Water Res.*, 2008, **42**, 4163.
36 O. Yamaguchi, J. Hidaka and K. Hirota, *J. Mater. Sci. Lett.*, 1991, **10**, 1471.
37 S. Inoue and S. Fujihara, *Inorg. Chem.*, 2011, **50**, 3605.
38 S. M. Zhang, G. K. Zhang, S. J. Yu, X. G. Chen and X. Y. Zhang, *J. Phys. Chem. C*, 2009, **113**, 20029.
39 G. T. Li, J. H. Qu, X. W. Zhang, H. J. Liu and H. N. Liu, *J. Mol. Catal. A: Chem.*, 2006, **259**, 238.
40 J. Bandara and J. Kiwi, *New J. Chem.*, 1999, **23**, 717.
41 W. J. Wang, L. Z. Zhang, T. C. An, G. Y. Li, H. Y. Yip and P. K. Wong, *Appl. Catal., B*, 2011, **108–109**, 108.
42 L. S. Zhang, K. H. Wong, H. Y. Yip, C. Hu, J. C. Yu, C. Y. Chan and P. K. Wong, *Environ. Sci. Technol.*, 2010, **44**, 1392.